

Proceedings of the International Conference on Oxide Materials for Electronic Engineering, May 29–June 2, 2017, Lviv

3D Computer Models of the Ag–Sb–Sn and MgO–Al₂O₃–SiO₂ $T-x-y$ Diagrams

V.I. LUTSYK^{a,b}, V.P. VOROB'YVA^a AND A.E. ZELENAYA^a

^aInstitute of Physical Materials Science (Siberian Branch of Russian Academy of Sciences),
Ulan-Ude, Russian Federation

^bBuryat State University, Ulan-Ude, Russian Federation

Three-dimensional (3D) computer models of Ag–Sb–Sn and MgO–Al₂O₃–SiO₂ systems $T-x-y$ diagrams have been designed. For the metal system two versions of 3D model of its phase diagram have been constructed according to the contradictions in the temperature intervals of the compound Sb₂Sn₃ stability. Possibilities of the analysis of the stages of crystallization and prediction of microstructural constituents with the aid of the calculation of vertical mass balance diagrams are demonstrated on the basis of the 3D computer model for the oxide system.

DOI: [10.12693/APhysPolA.133.763](https://doi.org/10.12693/APhysPolA.133.763)

PACS/topics: phase diagrams, 3D simulation, Ag–Sb–Sn, MgO–SiO₂–Al₂O₃, mass balance

1. Introduction

The study of the Ag–Sb–Sn system is connected with the creation of the lead-free solders. The MgO–SiO₂–Al₂O₃ system has wide practical application in the technology of the ceramic and glass-ceramic materials creation. It is used during the study and the description of the forsterite, periclase, spinel, corundum and mullite refractory materials. Its compounds, such as the forsterite 2MgO · SiO₂, the alumina-magnesia spinel MgO · Al₂O₃, the cordierite 2MgO · 2Al₂O₃ · 5SiO₂, have significant electrical insulating properties and are promising as thermoresistant ceramics [1–4].

Thermodynamic investigation methods of the metallic and ceramic systems are usually aimed to the solution of the applied problems, connected with the calculation of the thermodynamic and thermophysical properties [5–8]. But they do not give the possibility to restore the geometric structure of phase diagrams in total, whereas the assembling of 3D models from the phase regions makes it possible to obtain the complete model of phase diagram and to use it as a material-scientist tool for obtaining the data about the crystallization stages and the forming of microstructure constituents [9].

The universal description of all phase transformations within the ternary system can be obtained by its $T-x-y$ diagram 3D computer model [10, 11]. All available data are analyzed before the model construction. Usually this information is limited by binary systems, $x-y$ liquidus projection, table of phase's compositions, involved in the invariant reactions, by several isothermal sections and isopleths [5, 6, 12–14]. Then a scheme of the uni- and invariant states is constructed. This modernized Sheil' scheme is the excellent tool for "the conclusion" of the description of the $T-x-y$ diagram geometric structure in the tabular, and then in the 3D form. The 3D scheme of uni- and invariant states is the base of the $T-x-y$ diagram, which contains only three-phase regions (ruled surfaces) and isothermal (horizontal) planes, correspond-

ing to invariant transformations. The unruled surfaces of liquidus, solidus, solvus etc. finalize the $T-x-y$ construction. Final 3D model after the refinement of the curvature of unruled surfaces is possible to visualize in axonometric and $x-y$ projection, on any iso- and polythermal sections, and to obtain also the results of the calculations of the mass balances for any concentrations at any temperature [15]. In the case of essential divergences in the data of the different authors a 3D model is conveniently used for the results verification and for the resolving of the questionable moments [16].

2. 3D model of the Ag–Sb–Sn $T-x-y$ diagram

Each of three binary systems, which form the Ag–Sb–Sn system, has two incongruently melting compounds: R1, R2 in Ag–Sb, R3, R4 in Ag–Sn, R5, R6 in Sb–Sn; the only Sb₂Sn₃ = R6 is stoichiometric. The Ag–Sb–Sn=A–B–C system is characterized by three invariant quasi-peritectic reactions Q1: $L+B \rightarrow R2(R4)+R5$, Q2: $L+R5 \rightarrow R2(R4)+R6$, Q3: $L+R6 \rightarrow C+R2(R4)$ [12, 13] which involves the solid solution R2(R4). Another solid solution R1(R3) is formed by compounds R1 and R3.

The binary compound Sb₂Sn₃, represented in [12, 13], exists at room temperature (RT) (Fig. 1a). However, this compound decomposes at 242.4 °C in [5, 17] (Fig. 1b). Its existence is limited by the same temperature in the analogous system Ni–Sb–Sn [6], too. Therefore two schemes of uni- and invariant reactions are constructed (Fig. 2) for two versions of the binary system Sb–Sn (Fig. 1). Crystallization according to the first variant of the scheme (Fig. 2a) includes the ternary eutectoid reaction E: $C \rightarrow C1 + R2(R4) + R6$ with the participation of two allotropies of tin C and C1. Second version of the scheme (Fig. 2b) with the decomposition of the stoichiometric compound Sb₂Sn₃ = R6 into the solid solutions Sn = C and SbSn = R5 includes two eutectoid reactions E1: $C \rightarrow R2(R4) + R5 + R6$ and E2: $C \rightarrow C1 + R2(R4) + R5$.

Obviously, the 3D model is designed in two versions, too. The first one corresponds to [12–14], where the allotropy transformation passes as the eutectoid reaction E, and the 3D model consists of 99 surfaces and 62 phase regions (Fig. 3a). In another version with two eutectoid reactions E1 and E2, constructed according to [5, 17], the 3D model consists of 109 surfaces and 66 phase regions. Consequently, the conditions for the compound Sb_2Sn_3 existence require additional experimental study.

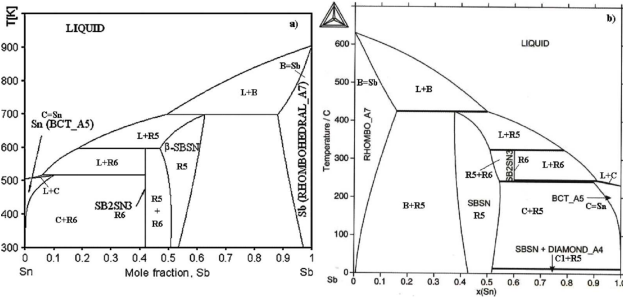


Fig. 1. Variants of the $T-x$ diagrams for the system Sb-Sn: [12] (a), [5] (b).

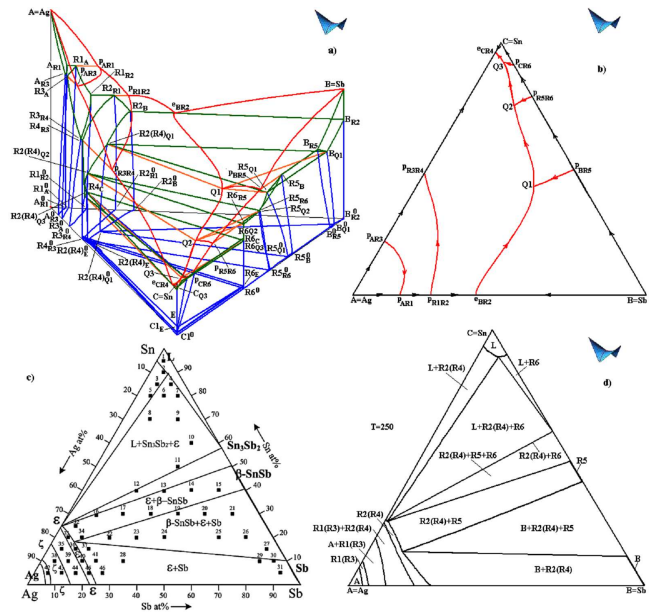


Fig. 3. 3D model of the Ag-Sb-Sn $T-x-y$ diagram (a), its liquidus $x-y$ projection (b), isothermal section at $T = 250$ °C: [12] (c), 3D model (d).

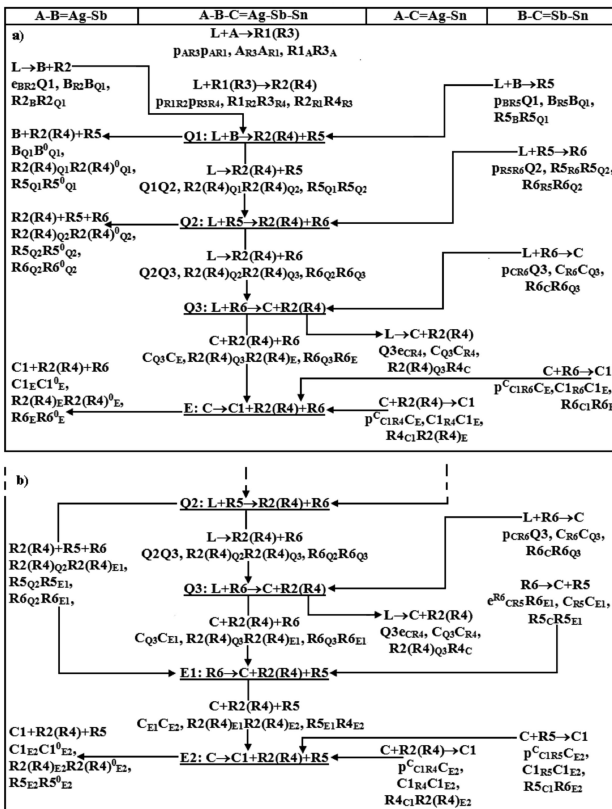


Fig. 2. Variants of the uni- and invariant states scheme according to versions of the binary system Sb-Sn: (a) Fig. 1a, (b) Fig. 1b.

The obtained 3D model makes it possible to analyze the $T-x-y$ diagram in the three-dimensional form or with the aid of any section. For instance, the model isothermal section at 250 °C (Fig. 3d) shows that Sb_2Sn_3 liquidus curve is missed in the analogous section in [12] and this curve is in the same section in [13], but the $L + b - SbSn$ phase region is indicated instead of the $L + Sn_3Sb_2$ region.

3. 3D model of the MgO-SiO₂-Al₂O₃ $T-x-y$ diagram

The MgO-SiO₂-Al₂O₃ (A-B-C) $T-x-y$ diagram has complicated geometrical construction. It includes four binary $R_1 = 2MgO \cdot SiO_2$, $R_2 = MgO \cdot SiO_2$, $R_3 = 3Al_2O_3 \cdot 2SiO_2$, $R_4 = MgO \cdot Al_2O_3$ and two ternary $R_5 = 4MgO \cdot 5Al_2O_3 \cdot 2SiO_2$, $R_6 = 2MgO \cdot 2Al_2O_3 \cdot 5SiO_2$ compounds; it is characterized by 11 invariant transformations: one peritectic $L_p + R_3 + R_4 \rightarrow R_5$, five quasi-peritectic $LQ_1 + R_4 \rightarrow R_1 + R_6$, $LQ_2 + R_5 \rightarrow R_4 + R_6$, $LQ_3 + R_3 \rightarrow R_5 + R_6$, $LQ_4 + C \rightarrow R_3 + R_4$, $LQ_5 + R_3 \rightarrow B_1 + R_6$, three eutectic $LE_1 \rightarrow A + R_1 + R_4$, $LE_2 \rightarrow R_1 + R_2 + R_6$, $LE_3 \rightarrow B_1 + R_2 + R_6$, two metatectic $B \rightarrow L_{V1} + B_1 + R_2$ and $B \rightarrow L_{V2} + B_1 + R_3$, corresponding to transfers from the high-temperature polymorphous modification of silica (B — cristobalite) to low-temperature one (B_1 — the tridymite) in the presence of liquid and compounds R_2 and R_3 [18, 19]. There is the immiscibility region of two melts beginning from the binary system MgO-SiO₂. Design of the 3D model took into account also three Van Rein' points in liquidus univariant curves $e_1 \in E_1Q_1$, $e_2 \in e_2e_3$ and $e_3 \in Q_3Q_5$.

The MgO-SiO₂-Al₂O₃ T - x - y diagram 3D model is formed by ten liquidus surfaces q , corresponding to primary crystallization of initial components MgO=A, Al₂O₃=C, two SiO₂ polymorphous modifications (B — cristobalite and B_1 — the tridymite) and six compounds $R1$ – $R6$. It includes also the liquid immiscibility surface i , 75 ruled surfaces as borders of two- and three-phase regions, 11 horizontal complexes at invariant points temperatures; it contains 21 two-phase and 30 three-phase regions (Fig. 4a). According to experimental data points V_1 and V_2 have the same temperature and the liquidus univariant curve V_1V_2 is located horizontally. Therefore the planes, which correspond to four-phase regroupings with the participation of the SiO₂ polymorphous modifications $B \rightarrow LV_1+B_1+R_2$ and $B \rightarrow LV_2+B_1+R_3$, are degenerated into the triangles $B_VV_1R_2V_1$ and $B_VV_2R_3V_2$, with the superposition of the four points B_{V1} , B_{1V1} , B_{V2} , B_{1V2} into the point B_V . In this case the phase region $L+B_1+B_2$ is degenerated into the plane $V_1V_2B_V$ and the univariant peritectic reaction $L^p+B \rightarrow B_1^p$, corresponding to it, occurs at constant temperature.

Projections of all geometric elements of the T - x - y diagram divide its concentration complex into 100 two-dimensional, 170 one-dimensional and 71 zero-dimensional concentration fields. In this case it is revealed that many concentration fields with the coinciding microstructure are located under the liquid immiscibility regions and the cristobalite liquidus surface. This is connected with the fact that the products of reactions taking place in the phase regions L_1+L_1 , L_1+L_1+B , $L+B$ are expanded in the earlier stages of crystallization and do not influence the total set of microstructure elements. It is also confirmed by the vertical mass balance diagrams (Fig. 4b).

Let us consider the mass center G (0.085, 0.808, 0.107) in the cristobalite liquidus field. It intersects 5 phase regions: $L+B$, $L+B+B_1$ (degenerated into the plane), $L+B_1$, $L+B_1+R_6$, $B_1+R_2+R_6$ with reactions as following: primary crystallization $L^1 \rightarrow B^1$; univariant peritectic reaction $L^p+B \rightarrow B_1^p$; post-peritectic primary crystallization $L^{1p} \rightarrow B_1^{1p}$; post-peritectic secondary eutectic reaction $L^{ep} \rightarrow B_1^{R2,ep} + R_6^{12,ep}$; invariant eutectic reaction $L^{E3} \rightarrow B_1^{E3} + R_2^{E3} + R_6^{E3}$ (Fig. 4b). Since the crystals B fully disappear as a result of reaction $L^p+B \rightarrow B_1^p$, they are not included in the set of micro-constituents. So the field in consideration is characterized by the following micro-constituents: B_1^p , B_1^{1p} , $B_1^{R2,ep}$, $R_6^{B2,ep}$, B_1^{E3} , R_2^{E3} , R_6^{E3} .

4. Conclusion

1. 3D computer models are the convenient tool for verification of data, represented in the different publications. Two variants of 3D model of the Ag-Sb-Sn T - x - y diagram have been constructed in accordance to two versions of existence/decomposition of the Sb₂Sn₃ compound. Furthermore, some inaccuracies in the isothermal section at 250 °C are discovered with their aid.

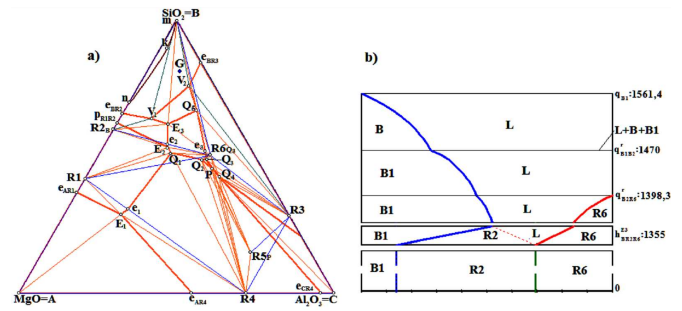


Fig. 4. x - y projection of the MgO-SiO₂-Al₂O₃ T - x - y diagram (a), the vertical mass balance diagram for the mass center G (0.085, 0.808, 0.107) (b).

2. The 3D computer model of the MgO-SiO₂-Al₂O₃ T - x - y diagram takes into account all topological features of its structure: cupola and immiscibility regions, Van Rein' points (e_1 , e_2 , e_3), allotropy of SiO₂, formation of six intermediate compounds. The model is used as a tool for study of crystallization schemes and microstructure prediction. It is established on its basis that the concentration fields in the boundaries of phase regions with the liquid immiscibility do not possess the unique sets of microstructure elements and their characteristics coincide with the concentration fields, located under the cristobalite liquidus.

Acknowledgments

This work has been performed under the program of fundamental research SB RAS (project 0336-2016-0006) and was partially supported by the Russian Foundation for Basic Research projects 15-43-04304, 16-48-030851, 17-08-00875.

References

- [1] V.Yu. Prokofjev, A.P. Ilyin, *Glass Ceram.* **9**, 14 (2004), (in Russian).
- [2] V.M. Pavlikov, E.P. Garmash, V.D. Tkachenko, I.V. Pleskach, B.K. Lupin, *Powder Metall. Met. Ceram.* **49**, 546 (2011).
- [3] Y. He, J.M. Guo, G.W. Zhang, X.L. Chen, J.C. Zhang, Z.L. Huang, G.Y. Liu, Q. Cai, *J. Ceram. Sci. Technol.* **6**, 201 (2015).
- [4] S.I. Shornikov, *Rus. J. Phys. Chem. A* **91**, 287 (2017).
- [5] A. Dinsdale, A. Watson, A. Kroupa, J. Vrestal, A. Zemanova, J. Vizdal, *Atlas of Phase Diagrams for Lead-Free Soldering*, Vol. 1, COST 531, European Science Foundation, Vydavatelstvi Knihar, Brno 2008.
- [6] A. Dinsdale, A. Kroupa, A. Watson, J. Vrestal, A. Zemanova, P. Broz, *COST MP0602-Handbook of High-Temperature Lead-Free Solders: Atlas of Phase Diagrams*, Vol. 1, COST, 2012.
- [7] I.-H. Jung, S.A. Decterov, A.D. Pelton, *J. Phase Equil. Diffus.* **25**, 329 (2004).
- [8] H. Maa, O. Fabrichnaya, M. Selleby, B. Sundman, *J. Mater. Res.* **20**, 975 (2005).

- [9] V. Lutsyk, A. Zelenaya, *J. Phys. Conf. Series* **790**, 012020 (2017).
- [10] V.I. Lutsyk, V.P. Vorob'eva, E.R. Nasrulin, *Crystallogr. Rep.* **54**, 1289 (2009).
- [11] V.I. Lutsyk, V.P. Vorob'eva, *Therm. Anal. Calorim.* **101**, 25 (2010).
- [12] S.-W. Chen, P.-Y. Chen, C.-N. Chin, Y.-C. Huang, C.-H. Wang, *Metall. Mater. Trans. A* **39a**, 3191 (2008).
- [13] W. Gierlotka, Y.-C. Huang, S.-W. Chen, *Metall. Mater. Trans. A* **39a**, 3199 (2008).
- [14] S.-W. Chen, C.-C. Chen, W. Gierlotka, *J. Electron. Mater.* **37**, 992 (2008).
- [15] V.I. Lutsyk, V.P. Vorob'eva, *Russ. J. Inorgan. Chem.* **61**, 188 (2016).
- [16] V.I. Lutsyk, V.P. Vorob'eva, S.Ya. Shodorova, *Russ. J. Inorgan. Chem.* **61**, 858 (2016).
- [17] A. Kroupa, J. Vizdal, *Def. Diff. Forum* **263**, 99 (2007).
- [18] E.M. Levin, C.R. Robbins, H.F. McMurdie, *Phase Diagrams for Ceramists*, American Ceramic Society, Ohio 1964.
- [19] N.A. Toropov, V.P. Bazarkovsky, V.V. Lapin, N.N. Kurtseva, A.I. Boykova, *Diagrams of Silicate Systems*, Vol. 3, *Ternary Silicate Systems*, Nauka, Leningrad 1972, (in Russian).